

# Constraining Lorentz Violation using 21cm and CMB Cross Correlations

**Bhuwan Joshi,<sup>a</sup> Rahul Kothari,<sup>a</sup> Shyam Chaudhary<sup>a</sup>**

<sup>a</sup>School of Physical Sciences, Indian Institute of Technology, Mandi, Himachal Pradesh, 175005

E-mail: [bhuwanj230@gmail.com](mailto:bhuwanj230@gmail.com), [quantummechanicskothari@gmail.com](mailto:quantummechanicskothari@gmail.com)

**Abstract.** Lorentz symmetry is a fundamental pillar of modern Physics, yet high-energy theories often predict its violation. One potential signature of such a violation is cosmic birefringence — rotation of the polarization plane of photons due to Chern-Simons coupling in Maxwell’s electrodynamics. This rotation angle, aka *birefringence angle*, depends upon the distance travelled by the photon and is thus different for CMB and 21cm photons. While the rotation angle in CMB, i.e.,  $\alpha_{\text{CMB}}$ , has been tightly constrained by CMB experiments, the potential of the 21cm cosmological signal to constrain this parameter, as well as constrain  $\alpha_{\text{21cm}}$ , remains largely unexplored. In this work, we provide constraints on both these angles by cross-correlating 21cm and CMB signals. Using the Fisher matrix formalism, we give our forecasts for 21cm experiments, including SKA, HIRAX, and PUMA, & Planck like CMB experiment. We find that best constraints  $\sigma_{\alpha_{\text{CMB}}} \sim 4.4^\circ$  and  $\sigma_{\alpha_{\text{21cm}}} \sim 100^\circ$  are found using  $C_\ell^{T_{21}B_{\text{CMB}}}$  and  $C_\ell^{T_{21}B_{21}}$  respectively. Since birefringence hasn’t yet been detected in 21cm, we choose the fiducial value  $\alpha_{\text{21cm}}^{\text{fid}} = 0$  assuming the null hypothesis.

---

## Contents

<b>1</b>	<b>Introduction</b>	<b>1</b>
<b>2</b>	<b>Modifying Maxwell Electrodynamics for testing Lorentz Violation</b>	<b>3</b>
<b>3</b>	<b>CMB and 21cm Line as cosmological probes</b>	<b>4</b>
3.1	CMB Temperature Anisotropies and Polarization	5
3.1.1	CMB Noise Power Spectra	5
3.2	Brightness Temperature and Polarization of 21cm Line	6
3.2.1	Instrumental Noise for 21cm Signal	7
<b>4</b>	<b>Cross Correlations for studying Lorentz Violation</b>	<b>8</b>
<b>5</b>	<b>Fisher Forecasts</b>	<b>9</b>
5.1	Effects of 21cm Foregrounds and Window Function	9
5.2	Results and Discussion	10
<b>6</b>	<b>Conclusion and Outlook</b>	<b>11</b>

---

## 1 Introduction

Lorentz invariance is one of the key ideas in Physics, according to which Physical laws should be consistent with Special Relativity, i.e., they should take the same form in all inertial frames that are boosted and/or rotated with respect to the frame in the picture. The standard model of particle Physics that describes three out of four fundamental interactions is based on QFTs, which are constructed to be Lorentz invariant from the beginning.

However, it is crucial to investigate places where Lorentz symmetry violation may take place. The fate of this symmetry at the most extreme energies of the universe remains one of the most pressing open questions in fundamental Physics. The investigation is interesting because quantum gravity theories suggest that Lorentz symmetry may not be a perfect symmetry of nature. Various approaches to quantum gravity, e.g., string theory [1, 2], loop quantum gravity [3, 4], spacetime noncommutativity [5], Horava Lifschitz gravity [6, 7], etc., often predict a minute breakdown of Lorentz invariance, typically at the Planck scale. The diffeomorphism invariance of General Relativity may be violated from spontaneous breaking of Lorentz symmetry, particularly in string theories [8, 9]. Consequently, hunting for the signatures of Lorentz violation is not merely a test of a foundational principle; it is also a direct experimental pathway to probe the quantum nature of gravity at Planck scales.

A broad spectrum of approaches, spanning highly controlled laboratory experiments to observations of high-energy cosmic particles, neutrinos, gamma rays, gravitational waves, etc., [9–15] have been carried out. Ref [9] uses 50 gravitational wave events and analyses anisotropic birefringence, whereas [14] solves the gravitational wave equation in the presence of Lorentz-violating terms. These results would be applicable in constraining symmetry violation with new gravitational wave detectors like LISA. Additionally, Ref [15] combines linear and circular polarization measurements of extragalactic sources for testing Lorentz violation. Interestingly, there have been suggestions to test Lorentz violation through blackhole Physics as well, e.g., by

observing the shadow cast by the Kerr-like black hole with or without plasma [16], analysing EHT observations under the purview of Horava gravity [17], etc.

Theoretically, the Lorentz violation manifests in modified theories of gravity, e.g., Horava-Lifshitz, Nieh-Yan, vector-tensor, Einstein Aether, bumblebee gravity, etc., [6, 7, 18–24]. In vector tensor theories of gravity, dynamical vector fields, besides the metric, are helpful to understand spontaneous Lorentz violation [19]. One specific case of vector tensor theory is the Einstein Aether theory, in which Lorentz invariance of General Relativity is broken by coupling a unit time-like vector field to the metric at every spacetime point [20, 21]. Particle physicists study Lorentz violation by going beyond standard model, where Lorentz violation is characterized by tensor-valued background fields which quantify the extent of symmetry violation by modified dispersion relations [11, 25]. In cosmology, the generalized bumblebee model [22–24] dynamically breaks Lorentz symmetry via a ‘bumblebee’ vector field ( $B_\mu$ ) that acquires a constant vacuum expectation value. Perturbations of this field are identified as the physical photon. A key consequence is that this ‘bumblebee photon’ propagates at a speed that is direction-dependent and different from the speed of ordinary matter, leading to testable effects in resonator and cosmic-ray experiments [22, 26].

In addition to these, a novel phenomenon occurs by introducing Chern-Simons term in Maxwell’s Lagrangian [10, 27]. This new term, in addition to breaking Lorentz symmetry, also causes parity violation. More importantly, it changes the EM dispersion relation, thereby implying *cosmic birefringence*, i.e., rotation of the plane of polarization of light as it travels over cosmological distances. A myriad of data sets have been employed to test the Lorentz violation signal by measuring this rotation angle. CMB experiments like WMAP, Planck, POLARBEAR, etc. [28–33], have set limits on how much rotation the CMB polarization could experience. A recent analysis of Planck data [31] reported a non-zero CMB birefringence angle  $0.35^\circ \pm 0.14^\circ$  (68% C.L.), (see also [32, 33]). The tightest constraints on Lorentz and CPT violation have been obtained using CMB polarization. Improvement in calibration accuracy in CMB would lead to an unambiguous measurement of parity and Lorentz violating effects [30]. Radio galaxies and quasar data have also been used in this regard [10]. Furthermore, the LSS galaxy survey analysis has reported an uncertainty of  $5^\circ - 15^\circ$  per galaxy [34] in galaxy birefringence angle. But the potential of next-generation 21cm intensity experiments to constrain Lorentz violation remains largely unexplored.

In this article, we constrain birefringence angles, both in CMB and 21cm signals (denoted respectively as  $\alpha_{\text{CMB}}$  and  $\alpha_{\text{21cm}}$ ) using their cross power spectra. We must mention that, 21cm signal has been cross correlated with other surveys, e.g., for testing local primordial non-gaussianities [35], cross correlation of CMB lensing and 21cm [36], cross correlation of 21cm and CMB polarizations [37] and so on. Most importantly, Ref [38] investigated cosmic birefringence by cross correlating 21cm temperature and CMB B-mode for probing Lorentz and parity violation by calculating the SNR in the reionization epochs. But to the best of our knowledge, no prior study pertaining to 21cm has constrained the birefringence angle in CMB or in 21cm. The present article serves this very purpose. From our analysis, we find that the best constraints  $\sigma_{\alpha_{\text{CMB}}} \sim 4.4^\circ$  and  $\sigma_{\alpha_{\text{21cm}}} \sim 100^\circ$  are found using  $C_\ell^{T_{21}B_{\text{CMB}}}$  and  $C_\ell^{T_{21}B_{21}}$  respectively. Such large uncertainties on  $\alpha_{\text{21cm}}$  is due to the weak 21cm polarization signal as compared to the instrumental noise. Since 21cm polarization hasn’t yet been detected, assuming the null hypothesis, we take  $\alpha_{\text{21cm}}^{\text{fid}} = 0$ .

The paper is organized as follows: in §2 we introduce basic Physics of cosmic birefringence when we add the Chern-Simons term to Maxwell’s Lagrangian. This leads to a modification of the photon dispersion relation, culminating in different rotations for left- and

right circular polarization. This is followed by a discussion of temperature and polarization modes of both CMB and 21cm & also their spherical harmonic coefficients in §3. We also discuss noise power spectra for both cases. These ideas are then applied in §4 to define cross correlations between CMB and 21cm signals. Then in §5, we present our Fisher forecasts while also discussing the effects of foregrounds and window function on our results. We conclude in §6. In this paper, we use fiducial  $\Lambda$ CDM cosmology with the best fit parameters from Planck 2018 paper [39]:  $h = 0.6766$ ,  $\Omega_b h^2 = 0.02242$ ,  $\Omega_c h^2 = 0.11933$ ,  $n_s = 0.9665$ ,  $A_s = 2.142 \times 10^{-9}$ .

## 2 Modifying Maxwell Electrodynamics for testing Lorentz Violation

We study Lorentz violation by modifying the electromagnetic Lagrangian, via adding a Chern-Simons term which involves a coupling of an external four-vector  $p^\mu$  with the dual of an electromagnetic field tensor  $\tilde{F}^{\mu\nu}$ . The gauge invariance then restricts the four-vector to be a constant [10]. The time component of  $p^\mu$  results in Lorentz violation, whereas the spatial components define a fixed direction in space, thereby breaking rotational invariance. Maxwell's Lagrangian, after adding the Chern-Simons term, becomes

$$\mathcal{L} = \mathcal{L}_{\text{EM}} + \mathcal{L}_{\text{CS}}, \quad \mathcal{L}_{\text{EM}} = -\frac{1}{4}F_{\mu\nu}F^{\mu\nu}, \quad \mathcal{L}_{\text{CS}} = -\frac{1}{2}p_\mu A_\nu \tilde{F}^{\mu\nu} \quad (2.1)$$

The field equations in the absence of sources, obtained after applying the Euler Lagrange equations on  $\mathcal{L}$  in (2.1) are

$$\partial_\alpha F^{\alpha\beta} = p_\mu \tilde{F}^{\mu\beta} \quad (2.2)$$

The source term appearing in the RHS of (2.2) is due to the topological charge density sourced by the Chern-Simons term. In terms of three vectors  $\mathbf{E}$  and  $\mathbf{B}$ , (2.2) gives the following modified forms of Gauss' and Ampere's laws (other equations remaining unchanged)

$$\nabla \cdot \mathbf{E} = -\mathbf{p} \cdot \mathbf{B} \quad (2.3)$$

$$\nabla \times \mathbf{B} = \frac{\partial \mathbf{E}}{\partial t} - p_0 B + \mathbf{p} \times \mathbf{E} \quad (2.4)$$

It can be noticed that by setting the vector  $p^\mu = 0$ , we get the standard source-free Maxwell's equations. To solve the modified equations, in (2.4), we substitute the following plane wave *ansatz*

$$\mathbf{E}(\mathbf{r}, t) = \mathbf{E}_0 e^{i(\mathbf{k} \cdot \mathbf{r} - \omega t)}, \quad \mathbf{B}(\mathbf{r}, t) = \mathbf{B}_0 e^{i(\mathbf{k} \cdot \mathbf{r} - \omega t)} \quad (2.5)$$

giving the solution for the  $\mathbf{E}$  field

$$(\omega^2 - k^2)\mathbf{E} + \mathbf{k}(\mathbf{k} \cdot \mathbf{E}) = i(p_0 \mathbf{k} - \omega \mathbf{p}) \times \mathbf{E} \quad (2.6)$$

To simplify further, we decompose the 3 vectors of the theory in the orthonormal system  $\hat{k}, \hat{e}_2$  and  $\hat{e}_3$ . In this triad, the spatial component of the four vector  $p^\mu = (p_0, \mathbf{p})$  can be written as  $\mathbf{p} = p_{||}\hat{k} + p_2\hat{e}_2 + p_3\hat{e}_3$ . In the same basis, (2.6) takes the following matrix form

$$\sum_j M_{ij} E_j = 0, \quad \text{where } M = \begin{pmatrix} \omega & -ip_3 & ip_2 \\ i\omega p_3 & \omega^2 - k^2 & i(p_0 k - \omega p_{||}) \\ -i\omega p_2 & -i(p_0 k - \omega p_{||}) & \omega^2 - k^2 \end{pmatrix} \quad (2.7)$$

Since this is a homogeneous system of equations, for a non-zero solution for  $\mathbf{E}$ , we must set  $\det M = 0$ . Thus, we get the modified dispersion relation

$$\omega^2 - k^2 = \pm (p_0 k - \omega |\mathbf{p}| \cos \theta) \left[ 1 - \frac{|\mathbf{p}|^2 \sin^2 \theta}{\omega^2 - k^2} \right]^{-1/2} \quad (2.8)$$

where  $\theta$  is the angle between the Chern-Simons vector  $\mathbf{p}$  and the wave vector  $\mathbf{k}$ . As a simple check, if we put  $p^\mu = 0$ , we get the standard dispersion relation back. The  $\pm$  signs in (2.8) correspond respectively to right and left-handed circularly polarized waves, indicating that the Chern-Simons modification to the electromagnetic Lagrangian, (2.1) leads to *birefringence*, i.e., different polarization states propagate with different phase velocities. Since Lorentz-violating effects are expected to be small, we only need to consider terms at linear order in the Lorentz-violating vector  $p^\mu$ . Thus (2.8) gives

$$k_\pm = \omega \mp \frac{1}{2}(p_0 - |\mathbf{p}| \cos \theta) \quad (2.9)$$

The phase change of either the left or right circularly polarized light as it travels a distance  $d$  is  $\phi_\pm = k_\pm \times d$ . The birefringence angle is then defined to be

$$\alpha = \frac{1}{2}(\phi_+ - \phi_-) = \frac{1}{2}(k_+ - k_-)d = -\frac{1}{2}(p_0 - |\mathbf{p}| \cos \theta)d \quad (2.10)$$

The rotation angle  $\alpha$  represents a measurable quantity that can be used to constrain Chern-Simons parameters  $p_0$  and  $\mathbf{p}$  through cosmological and astrophysical observations. We denote the birefringence angles in the case of CMB and 21cm, respectively, as  $\alpha_{\text{CMB}}$  and  $\alpha_{\text{21cm}}$ . Using Fisher analysis, together with the cross-correlations of 21cm and CMB, we put constraints on both these angles.

### 3 CMB and 21cm Line as cosmological probes

CMB has been an important probe for testing cosmological models. The radiation comprises photons that got decoupled out of cosmic plasma after the recombination era that happened around  $z \sim 1000$ . Before decoupling, the photons suffered Thomson scattering that gave rise to linear polarization. Thomson scattering is thus the primary cause of polarization in CMB radiation, in addition to having secondary effects like Sunyaev-Zel'dovich, which happens after reionization and affects polarization only at low multipoles. As the secondary effects in CMB are subdominant by at least one order of magnitude [40], in this study, we only focus our attention on primary effects.

Besides CMB, there are next-generation surveys of galaxy number counts, relying on the ability to resolve individual galaxies. This task progressively becomes harder as we go to higher redshifts. In such cases, observing the integrated emission of various lines like CO, HI, etc., is quite promising [41]. In particular, we have the 21cm line or HI that comes from neutral H, the most abundant element in the universe. The 21cm has found a lot of applications in studying cosmology – it has been used to investigate cosmic dark ages and cosmic dawn [42–44], to test general relativity and beyond [45–48], testing primordial anisotropies [49–51], constraining dark energy model parameters [52, 53], detectability of ultra-light axions particles [54], constraining inflation [55], detecting relativistic dipole [56] and so on.

### 3.1 CMB Temperature Anisotropies and Polarization

We give a brief summary of crucial results related to CMB (details can be found in [57, 58]), which also serves the purpose to set the notation. CMB (and also 21cm) radiation is characterized by Stokes vectors  $(I, Q, U)$ . Due to Thomson scattering, circular polarization  $V$  is absent [57]. However, there are some non-standard interactions that can generate the same in CMB, see [59–61]. For the purpose of this paper, we neglect the intrinsic circular polarization contribution due to these non-standard terms. For CMB,  $I = \Delta T(\hat{n})$ , i.e., temperature fluctuations, is the following dimensionless quantity

$$\Delta T(\hat{n}) = \frac{T_{\text{CMB}}(\hat{n})}{\bar{T}_{\text{CMB}}} - 1 \quad (3.1)$$

where  $T_{\text{CMB}}(\hat{n})$  is the CMB temperature measured along  $\hat{n}$ , over-bar throughout this paper denotes averaged quantities. Temperature fluctuations  $\Delta T$  behave as a scalar under rotation in the tangent plane along the line of sight  $\hat{n}$ . On the contrary, linear polarization components  $Q$  and  $U$  transform as

$$(Q \pm iU)'(\hat{n}) = e^{\mp 2i\psi}(Q \pm iU)(\hat{n}) \quad (3.2)$$

$\psi$  is the angle of rotation in the tangent plane. We thus use the  $\eth$  operator [62] to convert  $Q$  and  $U$  into rotationally invariant quantities known as  $E$  and  $B$  modes. Then we can perform spherical harmonic expansion

$$X_{\text{CMB}}(\hat{n}) = \sum_{\ell m} X_{\text{CMB},\ell m} Y_{\ell m}(\hat{n}) \quad (3.3)$$

where  $X \in \{\Delta T, E, B\}$ . On account of mathematical properties of  $\eth$  operator,  $\ell \geq 2$  when  $X \in \{B, E\}$ . Finally, we can relate the spherical harmonic coefficients with the primordial curvature perturbations  $\zeta(\mathbf{k})$  as

$$X_{\text{CMB},\ell m} = 4\pi i^\ell \int \frac{d^3 k}{(2\pi)^3} \Delta_{X,\ell}^{\text{CMB}}(k) Y_{\ell m}^*(\hat{k}) \zeta(\mathbf{k}) \quad (3.4)$$

where  $\Delta_{X,\ell}^{\text{CMB}}(k)$  are appropriate transfer functions calculated using CAMB software.

#### 3.1.1 CMB Noise Power Spectra

We give our forecasts assuming Planck-like CMB experiments. The noise power spectrum for CMB temperature anisotropy is [63]

$$N_\ell^{T_{\text{CMB}} T_{\text{CMB}}} = \left( \frac{\Delta_T}{\bar{T}_{\text{CMB}}} \right)^2 \exp \left( \frac{\ell(\ell+1)\theta_{\text{FWHM}}^2}{8 \ln 2} \right) \quad (3.5)$$

where  $\Delta_T = 1 \mu\text{K-arcmin}$  represents the thermal noise sensitivity and  $\theta_{\text{FWHM}}$  denotes the full width at half maximum (FWHM) of the beam. For this analysis, we adopt  $\theta_{\text{FWHM}} = 5 \text{ arcmin}$  [64]. For the E and B modes, the noise power spectrum can be written as [65]

$$N_\ell^{E_{\text{CMB}} E_{\text{CMB}}} = N_\ell^{B_{\text{CMB}} B_{\text{CMB}}} = 2N_\ell^{T_{\text{CMB}} T_{\text{CMB}}} \quad (3.6)$$

### 3.2 Brightness Temperature and Polarization of 21cm Line

The 21cm line corresponds to the hyperfine transition between two closely spaced energy levels of the H atom known as *singlet* and *triplet* states. For the 21cm line,  $I$  component of Stokes vector is the excess brightness temperature relative to the CMB, expressed as [66–68]

$$\delta T_b(\hat{n}, z) = \frac{T_S - T_{\text{CMB}}(\hat{n})}{1 + z} \tilde{\tau} \quad (3.7)$$

where the spin temperature  $T_S$  decides the relative abundance of singlet and triplet states and  $\tilde{\tau} \ll 1$  is the optical depth. Using  $\delta T_b(\hat{n}, z)$ , we can define dimensionless 21cm brightness contrast in the Fourier space as

$$\delta_{\text{HI}}(\mathbf{k}, z) \equiv \frac{\delta T_b(\mathbf{k}, z)}{\delta T_b(z)} - 1 = (b_{21}(z) + \mu^2 f(z)) \delta_m(\mathbf{k}, z) \quad (3.8)$$

here  $\mu = \hat{k} \cdot \hat{n}$ ,  $\hat{n}$  is the line of sight,  $f$  is the linear growth rate related to growth factor  $D$  by  $f = d \ln D(a) / d \ln a$ . The first term is the HI density contrast, related to dark matter density contrast  $\delta_m(k, z)$  through the bias parameter  $b_{21}$ . Since the majority of neutral hydrogen is found in self-shielded gas clouds inside galaxies in later times, the hydrogen density field is a biased indicator of the dark matter density field related through the bias. The second term corresponds to the redshift-space distortions [69]. We also have 21cm polarization, first studied by Babich and Loeb [70]. It can probe the epoch of reionization. The linear polarization is produced through two mechanisms: (a) intrinsic characteristics of the sources and (b) secondary processes. In so far as the circular polarization is concerned, it arises from the interaction between the local quadrupole moment of the hydrogen atoms and anisotropies in the CMB radiation field, which induces a net spin orientation in the neutral hydrogen population. Just like CMB, we assume it to be small and thus neglect it for the purpose of our paper.

Using the standard line-of-sight integration method, we can get spherical harmonic coefficients for 21cm brightness temperature and polarization [70, 71]

$$X_{21,\ell m}(z) = 4\pi i^\ell \int \frac{d^3 \mathbf{k}}{(2\pi)^3} \Delta_{X,\ell}^{21}(k, z) Y_{\ell m}^*(\hat{k}) \delta_m(\mathbf{k}, z) \quad (3.9)$$

with the difference that in (3.4), the harmonic coefficients didn't have any  $z$  dependence. In (3.9), the 21cm brightness temperature transfer functions for T and E modes are (adapted from [71])

$$\Delta_{T,\ell}^{21}(k, z) = b_{21}(z) j_\ell(kr) - f(z) j_\ell''(kr), \quad (3.10)$$

$$\begin{aligned} \Delta_{E,\ell}^{21}(k, z) = & \frac{3}{4} \sqrt{\frac{(\ell+2)!}{(\ell-2)!}} \left[ b_{21}(z) \int_\eta^{\eta_0} d\eta' g(\eta') j_2[k(\eta' - \eta)] \frac{j_\ell[k(\eta_0 - \eta')]}{[k(\eta_0 - \eta')]^2} \right. \\ & \left. - f(z) \int_\eta^{\eta_0} d\eta' g(\eta') j_2''[k(\eta' - \eta)] \frac{j_\ell[k(\eta_0 - \eta')]}{[k(\eta_0 - \eta')]^2} \right] \end{aligned} \quad (3.11)$$

where again  $\ell \geq 2$  for E mode in (3.11). Here we should point out that auto power spectra  $B_{21}B_{21}$  come in covariance along with the noise power spectrum (c.f. (5.2)). Also, since  $B_{21}B_{21}$  power is expected to be small as compared to instrumental noise, so we don't really need an expression for this correlation. Also,  $r(z) = \eta(0) - \eta(z)$  is the conformal distance to

	HIRAX-1024	PUMA	SKA-Mid
Redshift range	0.775 – 2.55	0.3 – 6.0	0.35 – 3.05
Integration time, $t_{\text{survey}}$ (sec)	$1.58 \times 10^8$	$1.58 \times 10^8$	$3.6 \times 10^7$
Sky fraction, $f_{\text{sky}}$	0.36	0.5	0.49
Dish diameter, $D_{\text{dish}}$ (m)	6	6	15
Maximum baseline	0.25 km	1.0 km	150 km
$N_{\text{dish}}$	1,024	32,000	197

**Table 1.** The instrumental details of the HIRAX-1024 and PUMA radio interferometers used in this work [78, 79]. Information about SKA-Mid (Band 1) is based on data from the official website [SKA-MID](#).

a point at redshift  $z$ . The integration limit in (3.11) is from the emitted conformal time  $\eta$  to the present time  $\eta_0$ . Also, the visibility function is defined as  $g(\eta) = (d\tau/d\eta)e^{-\tau}$  and  $\tau$  being the Thomson scattering optical depth [72]

$$\tau(\eta) = \int_{\eta}^{\eta_0} \frac{\sigma_T n_b x_e(\eta')}{a(\eta')^2} d\eta'. \quad (3.12)$$

Here  $n_b$  is the baryon comoving number density (equivalent to the present physical number density),  $\sigma_T$  is the Thomson scattering total cross section and  $x_e(\eta)$  is the mean ionisation fraction [72]

$$x_e(z) = \frac{1}{2} \left\{ 1 - \tanh \left[ \frac{y(z) - y_{\text{re}}}{\Delta_y} \right] \right\} \quad (3.13)$$

with  $y(z) = (1+z)^{3/2}$ ,  $\Delta_y$  and  $y_{\text{re}}$  are the reionization model parameters.

### 3.2.1 Instrumental Noise for 21cm Signal

We consider radio telescopes operating in two distinct modes – (a) single-dish (hereafter SD), in which we sum over auto correlations from all dishes and (b) interferometer (IF henceforth), where the cross correlations are combined. SD mode captures larger angular scales, whereas IF is adapted for relatively smaller ones. In this paper, we work with SKA-MID in SD and HIRAX & PUMA in IF modes. For 21cm mapping, the dominant noise, relevant to the scales of interest, is due to the instrument, while the shot noise contribution is subdominant [73–76]. We can write the temperature noise power spectrum for both SD and IF in a single formula as [72, 77]

$$N_{\ell}^{T_{21}T_{21}}(z) = \frac{2\pi f_{\text{sky}} T_{\text{sys}}^2(z)}{t_{\text{survey}} B(z) (\delta \bar{T}_b(z))^2} \frac{\alpha_{\ell}(z)}{\beta_{\ell}^2(z)} \quad (3.14)$$

where  $T_{\text{sys}}$  is the system temperature,  $t_{\text{survey}}$  the total observation time, the bandwidth  $B(z) = \nu_{21} \Delta z / (1+z)^2$ ,  $\delta \bar{T}_b(z)$  the mean background 21cm brightness temperature,  $\alpha_{\ell}$  the dish density factor and  $\beta_{\ell}$  the effective beam. Expressions for these are given in [77]. Similar to CMB (c.f. (3.6)), we consider the noise power spectra

$$N_{\ell}^{E_{21}E_{21}} = 2N_{\ell}^{T_{21}T_{21}} \quad (3.15)$$

## 4 Cross Correlations for studying Lorentz Violation

The spherical harmonic coefficients of  $T$ ,  $E$  and  $B$  modes, under parity transform as

$$T_{\ell m} \rightarrow (-1)^\ell T_{\ell m}, \quad E_{\ell m} \rightarrow (-1)^\ell E_{\ell m}, \quad B_{\ell m} \rightarrow (-1)^{\ell+1} B_{\ell m} \quad (4.1)$$

These properties hold for both CMB and 21cm signals. By ensemble average of spherical harmonic coefficients, we can define the angular power spectra

$$\langle X_{\ell m}^a (Y_{\ell' m'}^b)^* \rangle = \delta_{\ell \ell'} \delta_{mm'} C_\ell^{X_a Y_b} \quad (4.2)$$

where  $X, Y \in \{\Delta T, E, B\}$  denote the mode being considered and  $a, b \in \{\text{CMB}, 21\text{cm}\}$ , the corresponding signal. The harmonic coefficients can have redshift dependences (e.g., for the 21cm case) that we don't show explicitly for notational brevity. The Kronecker deltas arise from statistical isotropy. As the power spectra is parity invariant, it follows that the cross correlation of  $B$  mode of either CMB or 21cm with the remaining fields is zero, i.e.,  $C_\ell^{X_a B_b} = 0$  for  $X \neq B$ , e.g.,  $C_\ell^{T_{21} B_{21}} = C_\ell^{E_{\text{CMB}} B_{21}} = 0$ , etc. However, this is no longer true in the presence of birefringence, where mixing of  $E$  and  $B$  modes takes place, and thus we can write [80]

$$T_{a, \ell m}^O = T_{a, \ell m} \quad (4.3)$$

$$E_{a, \ell m}^O = E_{a, \ell m} \cos(2\alpha_a) - B_{a, \ell m} \sin(2\alpha_a) \quad (4.4)$$

$$B_{a, \ell m}^O = E_{a, \ell m} \sin(2\alpha_a) + B_{a, \ell m} \cos(2\alpha_a) \quad (4.5)$$

where again  $a \in \{\text{CMB}, 21\text{cm}\}$  and “O” in the superscript denotes the harmonic coefficients in the presence of birefringence. Thus, in the presence of birefringence,  $E$  and  $B$  modes are mixed; however, the  $T$  mode remains unaffected. This is true for both 21cm and CMB signals. Clearly,  $\alpha_{\text{CMB}} \neq \alpha_{21\text{cm}}$  as the photons in the two cases will travel different distances and thus will have different birefringence angles. In the presence of birefringence, we define the cross power spectra just like in (4.2) as

$$\langle X_{a, \ell m}^O (Y_{b, \ell' m'}^O)^* \rangle = \delta_{\ell \ell'} \delta_{mm'} C_\ell^{X_a Y_b, O} \quad (4.6)$$

Using (4.4) and (4.5), together with the definition (4.6), it follows that

$$C_\ell^{T_a B_b, O} = C_\ell^{T_a E_b} \sin(2\alpha_b) \quad (4.7)$$

$$C_\ell^{E_a B_b, O} = C_\ell^{E_a E_b} \sin(2\alpha_b) \cos(2\alpha_a) - C_\ell^{B_a B_b} \sin(2\alpha_a) \cos(2\alpha_b) \quad (4.8)$$

We can simplify these expressions by noting that (a) the birefringence angles are small, i.e.  $\alpha_a \ll 1$ , and (b) B-mode power spectra are small as compared with E-mode, which gives

$$C_\ell^{T_a B_b, O} = 2\alpha_b C_\ell^{T_a E_b} \quad (4.9)$$

$$C_\ell^{E_a B_b, O} = 2\alpha_b C_\ell^{E_a E_b} \quad (4.10)$$

From (4.9) and (4.10), it is clear that the angles  $\alpha_{\text{CMB}}$  and  $\alpha_{21\text{cm}}$  don't couple and thus we can constrain them separately. This means our Fisher Matrix takes a diagonal form. For our analysis, we consider the fiducial value of the CMB birefringence angle  $\alpha_{\text{CMB}}^{\text{fid}} = 0.3^\circ$  as has been used by Planck [32]. As the birefringence hasn't yet been detected in 21cm radiation, we constrain  $\alpha_{21\text{cm}}$  adopting the null hypothesis and consider  $\alpha_{21\text{cm}}^{\text{fid}} = 0$ .

We now enumerate all possible cross-correlations between CMB and 21cm signals that can be used to constrain  $\alpha_a$ . Since one of the fields in the cross correlation has to be the B mode (either from 21cm or CMB), we have 8 possibilities – out of these,  $E_{\text{CMB}}B_{\text{CMB}}$  and  $T_{\text{CMB}}B_{\text{CMB}}$  have already been considered for constraining  $\alpha_{\text{CMB}}$  by Planck [81]. So we give our constraints using – (a)  $T_{21}B_{21}$  (b)  $E_{21}B_{21}$  (c)  $E_{\text{CMB}}B_{21}$  (d)  $T_{\text{CMB}}B_{21}$  (e)  $E_{21}B_{\text{CMB}}$  and (f)  $T_{21}B_{\text{CMB}}$ . Thus first four correlations are used to put constraints on  $\alpha_{\text{21cm}}$  while the last two are used to constrain  $\alpha_{\text{CMB}}$ .

## 5 Fisher Forecasts

We define our Fisher matrix as [65]

$$F_{\alpha_a \alpha_b}^{X_a Y_b}(z) = \sum_{\ell=\ell_{\min}}^{\ell_{\max}} \frac{\partial C_{\ell}^{X_a Y_b, \text{O}}}{\partial \alpha_a} \frac{\partial C_{\ell}^{X_a Y_b, \text{O}}}{\partial \alpha_b} \frac{1}{\text{Cov}(\tilde{C}_{\ell}^{X_a Y_b, \text{O}}, \tilde{C}_{\ell}^{X_a Y_b, \text{O}})} \quad (5.1)$$

where  $F_{\alpha_a \alpha_b}^{X_a Y_b}$  is the Fisher matrix element obtained using the cross correlation  $C_{\ell}^{X_a Y_b}$ . The covariance, on account of the fact that birefringence angles in (4.4) & (4.5) are small, and thus we need to keep only  $\mathcal{O}(\alpha_a)$  terms, can be written as

$$\text{Cov}(\tilde{C}_{\ell}^{X_a Y_b, \text{O}}, \tilde{C}_{\ell}^{X_a Y_b, \text{O}}) \approx \frac{1}{(2\ell+1)f_{\text{sky}}} \left( \tilde{C}_{\ell}^{X_a X_a} \tilde{C}_{\ell}^{Y_b Y_b} + \left( \tilde{C}_{\ell}^{X_a Y_b, \text{O}} \right)^2 \right) \quad (5.2)$$

where quantity with tilde represents the noise added angular power spectrum. Following [65], we consider a zero noise power spectrum for cross-correlations between different fields and signals. For auto correlation, the expressions for noise power spectra  $N_{\ell}^{X_{\text{CMB}} X_{\text{CMB}}}$  with  $X \in \{\Delta T, E, B\}$  are given in (3.5) and (3.6) while that for 21cm in (3.14) and (3.15). Finally,  $\ell$  in (5.1) ranges over values that depend upon both (a) redshift  $z$  and (b) the survey mode being employed. The accessible multipoles for single-dish (SD) and interferometer (IF) modes are [82]

$$\ell_{\min}(z) = \begin{cases} 2 & \text{SD} \\ 150/(1+z) & \text{IF} \end{cases}, \quad \ell_{\max}(z) = \begin{cases} 450/(1+z) & \text{SD} \\ 500 & \text{IF} \end{cases} \quad (5.3)$$

Leveraging the tomographic nature of intensity mapping experiments, we compute the total Fisher information by summing over independent redshift bins,  $F_{\alpha_a \alpha_b, \text{tot}}^{X_a Y_b} = \sum_{z_i} F_{\alpha_a \alpha_b}^{X_a Y_b}(z_i)$  in the corresponding redshift range. Since the Fisher matrix is diagonal, we define

$$\sigma_{\alpha_a} = \left( F_{\alpha_a \alpha_a, \text{tot}}^{X_b Y_a} \right)^{-1/2} \quad (5.4)$$

using cross correlation  $C_{\ell}^{X_b Y_a}$ . Following [79, 83, 84], we use redshift bin width  $\Delta z = 0.1$ . Also, as was discussed in the previous section, we use  $\alpha_{\text{CMB}}^{\text{fid}} = 0.3^\circ$  and  $\alpha_{\text{21cm}}^{\text{fid}} = 0$

### 5.1 Effects of 21cm Foregrounds and Window Function

Before presenting our results in the next section, we'd like to discuss the effects of foregrounds and window functions on our constraints. It is well known that foreground levels in 21cm are 5 orders of magnitude higher than the signal [85–87], thereby playing an important role in auto power and bispectrum estimation. It is also a very well-known fact that contaminants of individual surveys are biased, thus they don't affect cross correlation (see [55, 88, 89] and

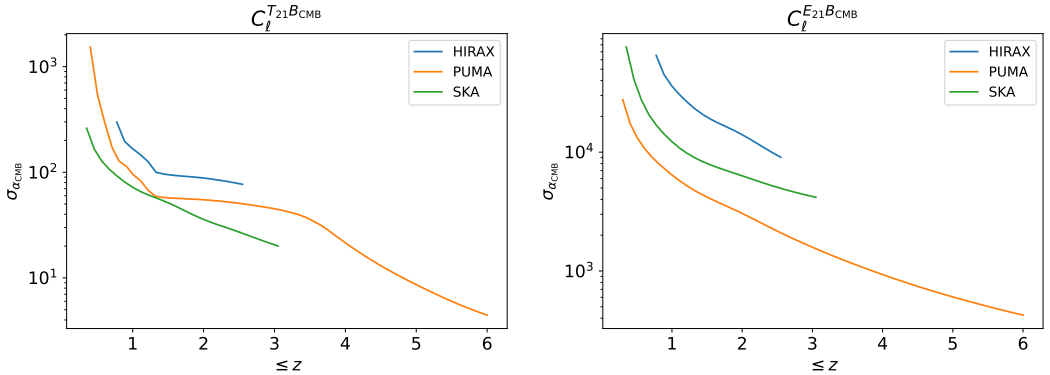


**Figure 1.** Cumulative error on the birefringence angle  $\alpha_{\text{CMB}}$  (in degrees) as a function of redshift using various correlations. In these plots, we have used  $\alpha_{\text{CMB}}^{\text{fid}} = 0.3^\circ$ . The bin-width for the Dirac window function is chosen to be  $\Delta z = 0.1$ . The correlations considered are left:  $C_{\ell}^{T_{21}B_{\text{CMB}}}$  and right:  $C_{\ell}^{E_{21}B_{\text{CMB}}}$ . It is clear that  $C_{\ell}^{T_{21}B_{\text{CMB}}}$  gives the best constraint on  $\alpha_{\text{CMB}}$ .

references therein). So it might appear that foregrounds play no role in covariance for cross-correlation. However, from (5.2), it is clear that even for cross correlations, the covariance term contains auto power spectra like  $C_{\ell}^{T_{21}T_{21}}$  and  $C_{\ell}^{E_{21}E_{21}}$ . Now we assess the effect of foregrounds on our constraints. Since foregrounds contaminate only large angular scales, their effects are considered by the cut  $\ell_{\text{min}}^{\text{fg}} \geq 5$  [77]. However, from (5.3), we find that  $\ell_{\text{min}} \geq 20$  for all the redshifts considered in this paper. Thus, we conclude that foreground effects on  $C_{\ell}^{T_{21}T_{21}}$  don't alter our constraints for surveys in IF modes (PUMA and HIRAX). But they definitely play an important role, albeit very small, when we consider surveys in SD mode (SKA-Mid). For 21cm polarization, the instrumental noise is orders of magnitude higher than  $C_{\ell}^{E_{21}E_{21}}$ . We expect that since foregrounds will only reduce this signal even further, there will be no effect of foregrounds in this case, too. We give our constraints considering all these facts into consideration.

We now turn our attention to the window function. Although the tophat function is more realistic for making comparisons with the observations, we found that using a Dirac window in place of tophat doesn't change the results significantly. E.g., considering PUMA and  $C_{\ell}^{T_{21}B_{\text{CMB}}}$ , we find  $\sigma_{\alpha_{\text{CMB}}} 3.18^\circ$  and  $4.42^\circ$  respectively for tophat and Dirac windows. Thus, to avoid numerical complications, for all subsequent analysis, we use the Dirac window function.

## 5.2 Results and Discussion

We present the Fisher matrix forecasts using various experiments – SKA, HIRAX, and PUMA.

1. In Figure 1, we give our constraints for  $\alpha_{\text{CMB}}$ . The best constraints  $\sigma_{\alpha_{\text{CMB}}} \sim 4^\circ$  on  $\alpha_{\text{CMB}}$  are obtained using  $C_{\ell}^{T_{21}B_{\text{CMB}}}$ . This is due to the fact that the 21cm brightness temperature signal is larger as compared with  $E_{21}$ . This results in large covariance and hence better constraints.
2. Constraints provided by  $C_{\ell}^{T_{21}B_{\text{CMB}}}$  are less competitive than the CMB-only limits, e.g., [32, 33]. This can be attributed to the weak correlation between 21cm and CMB signals, which further happens due to the large redshift separation between the primary CMB from the surface of last scattering and the 21cm signal in the post-reionisation epoch.

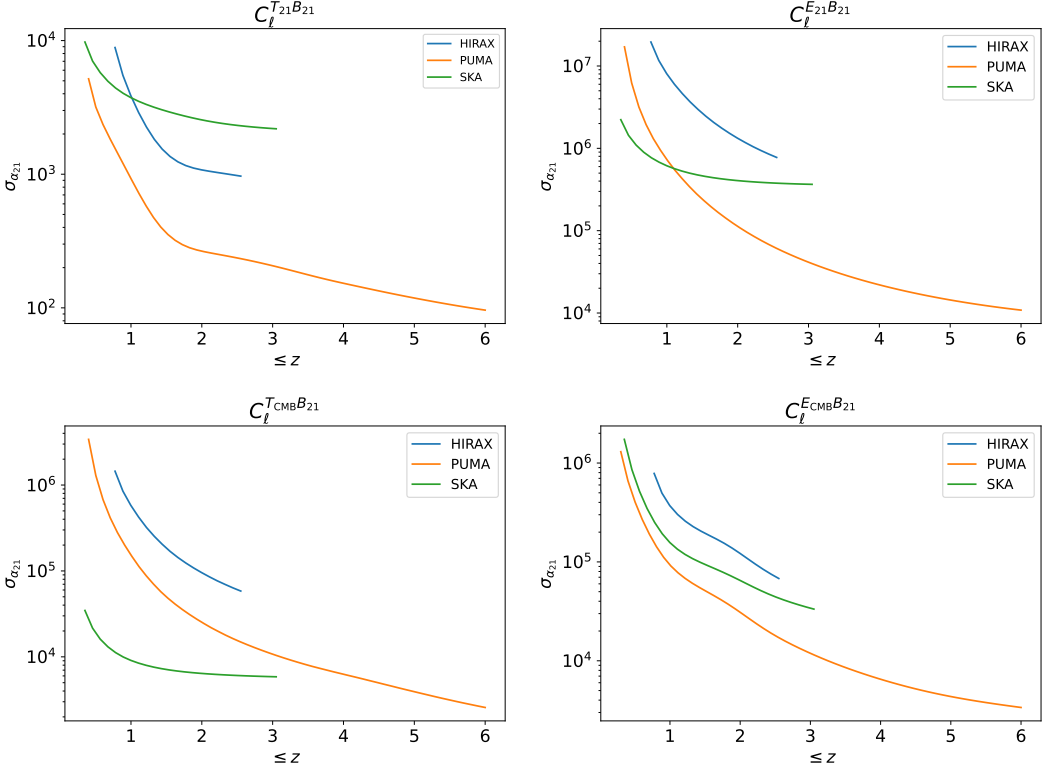


**Figure 2.** Cumulative error on birefringence angle  $\alpha_{21\text{cm}}$  (in degrees) as a function of redshift using various correlations. Here, we've used  $\alpha_{21\text{cm}}^{\text{fid}} = 0$  (for discussion, see §4). *Row 1:* left  $C_{\ell}^{T_{21}B_{21}}$  and right:  $C_{\ell}^{E_{21}B_{21}}$ , *Row 2:* left:  $C_{\ell}^{T_{\text{CMB}}B_{21}}$  and right:  $C_{\ell}^{E_{\text{CMB}}B_{21}}$ . It is clear that  $C_{\ell}^{T_{21}B_{21}}$  has the best constraining power out of all possibilities.

3. In Figure 2, we give constraints on  $\alpha_{21\text{cm}}$ . The best constraints  $\sigma_{\alpha_{21\text{cm}}} \sim 100^\circ$  are obtained using  $C_{\ell}^{T_{21}B_{21}}$ . Such a poor constraint is due to a weak 21cm polarization signal as compared to the instrumental noise. We are optimistic that in the near future, once next-generation instrumentation reduces the noise levels even further, more stringent constraints will become achievable. Future experiments achieving significantly lower thermal noise levels may unlock the potential of the 21cm E-mode.

## 6 Conclusion and Outlook

In this study, we gave constraints on birefringence angles  $\alpha_{\text{CMB}}$  and  $\alpha_{21\text{cm}}$  using futuristic 21cm and Planck-like CMB experiments. Our results indicate that if we cross-correlate the 21cm brightness temperature with the CMB, we can constrain the birefringence angle  $\alpha_{\text{CMB}} = 0.3 \pm 4.4^\circ$  for the integrated PUMA experiment, though we don't get good constraints on  $\alpha_{21\text{cm}}$ , where we get  $\sigma_{\alpha_{21}} \approx 100^\circ$ . We found that the best constraints on these angles are given by cross correlations  $C_{\ell}^{T_{21}B_{\text{CMB}}}$  and  $C_{\ell}^{T_{21}B_{21}}$  respectively. We further found that the constraints obtained on  $\alpha_{\text{CMB}}$  aren't as good as those obtained before using CMB-only limits. We believe that it is due to weaker cross correlation between 21cm and CMB signals (compared to what happens in CMB only case), which further happens due to large redshift separation.

## Acknowledgments

Rahul Kothari acknowledges computing facilities availed through the IIT Mandi seed Grant IITM/SG/DIS-ROS-SPA/111. We are also truly thankful to Eiichiro Komatsu for the discussions.

## References

- [1] V. A. Kostelecky and S. Samuel, *Spontaneous Breaking of Lorentz Symmetry in String Theory*, *Phys. Rev. D* **39** (1989) 683.
- [2] N. E. Mavromatos, *Lorentz Invariance Violation from String Theory*, *PoS QG-PH* (2007) 027 [[0708.2250](#)].
- [3] R. Gambini and J. Pullin, *Nonstandard optics from quantum space-time*, *Phys. Rev. D* **59** (1999) 124021 [[gr-qc/9809038](#)].
- [4] H. Vucetich, *Testing Lorentz invariance violation in quantum gravity theories*, [gr-qc/0502093](#).
- [5] S. M. Carroll, J. A. Harvey, V. A. Kostelecky, C. D. Lane and T. Okamoto, *Noncommutative field theory and Lorentz violation*, *Phys. Rev. Lett.* **87** (2001) 141601 [[hep-th/0105082](#)].
- [6] P. Horava, *Quantum Gravity at a Lifshitz Point*, *Phys. Rev. D* **79** (2009) 084008 [[0901.3775](#)].
- [7] A. Wang, *Hořava gravity at a Lifshitz point: A progress report*, *Int. J. Mod. Phys. D* **26** (2017) 1730014 [[1701.06087](#)].
- [8] C. M. Reyes and M. Schreck, *Modified-gravity theories with nondynamical background fields*, *Phys. Rev. D* **106** (2022) 044050 [[2202.11881](#)].
- [9] Z. Wang, L. Shao and C. Liu, *New Limits on the Lorentz/CPT Symmetry Through 50 Gravitational-wave Events*, *Astrophys. J.* **921** (2021) 158 [[2108.02974](#)].
- [10] S. M. Carroll, G. B. Field and R. Jackiw, *Limits on a Lorentz and Parity Violating Modification of Electrodynamics*, *Phys. Rev. D* **41** (1990) 1231.
- [11] D. Amram, K. Bouzoud, N. Chanon, H. Hansen, M. R. Ribeiro, Jr. and M. Schreck, *New Constraint for Isotropic Lorentz Violation from LHC Data*, *Phys. Rev. Lett.* **132** (2024) 211801 [[2312.11307](#)].
- [12] F. W. Stecker, *Chapter 12: Testing Lorentz Invariance with Neutrinos*, in *The Encyclopedia of Cosmology*, G. G. Fazi, ed., pp. 579–610, (2023), [2202.01183](#), DOI.
- [13] H. Li and B.-Q. Ma, *Threshold anomalies of ultra-high energy cosmic photons due to Lorentz invariance violation*, *JHEAp* **32** (2021) 1 [[2105.06647](#)].
- [14] S. Aoulad Lafkih, M.-C. Angonin, C. Le Poncin-Lafitte and N. A. Nilsson, *Gravitational-wave generation in the presence of Lorentz invariance violation*, [2506.08859](#).
- [15] R. Gerasimov, P. Bhoj and F. Kislat, *New Constraints on Lorentz Invariance Violation from Combined Linear and Circular Optical Polarimetry of Extragalactic Sources*, *Symmetry* **13** (2021) 880 [[2104.00238](#)].
- [16] H.-M. Wang and S.-W. Wei, *Shadow cast by Kerr-like black hole in the presence of plasma in Einstein-bumblebee gravity*, *Eur. Phys. J. Plus* **137** (2022) 571 [[2106.14602](#)].
- [17] W. Liu, H. Huang, D. Wu and J. Wang, *Lorentz violation signatures in the low-energy sector of Hořava gravity from black hole shadow observations*, *Phys. Lett. B* **868** (2025) 139812 [[2506.13504](#)].
- [18] R.-G. Cai, C. Fu and W.-W. Yu, *Parity violation in stochastic gravitational wave background from inflation in Nieh-Yan modified teleparallel gravity*, *Phys. Rev. D* **105** (2022) 103520 [[2112.04794](#)].

- [19] V. H. Satheeshkumar, *Nature of singularities in vector-tensor theories of gravity*, in *16th Marcel Grossmann Meeting on Recent Developments in Theoretical and Experimental General Relativity, Astrophysics and Relativistic Field Theories*, 11, 2021, DOI [\[2111.03066\]](#).
- [20] M. M. Ivanov, *Cosmological constraints on Lorentz Invariance violation in gravity and dark matter*, in *51st Rencontres de Moriond on Cosmology*, pp. 237–240, 5, 2016, [1605.04168](#).
- [21] J. Oost, S. Mukohyama and A. Wang, *Spherically Symmetric Exact Vacuum Solutions in Einstein-Aether Theory*, *Universe* **7** (2021) 272 [\[2106.09044\]](#).
- [22] M. D. Seifert, *Generalized bumblebee models and Lorentz-violating electrodynamics*, *Phys. Rev. D* **81** (2010) 065010 [\[0909.3118\]](#).
- [23] R. Bluhm and V. A. Kostelecky, *Spontaneous Lorentz violation, Nambu-Goldstone modes, and gravity*, *Phys. Rev. D* **71** (2005) 065008 [\[hep-th/0412320\]](#).
- [24] R. Bluhm, S.-H. Fung and V. A. Kostelecky, *Spontaneous Lorentz and Diffeomorphism Violation, Massive Modes, and Gravity*, *Phys. Rev. D* **77** (2008) 065020 [\[0712.4119\]](#).
- [25] D. Colladay and V. A. Kostelecky, *Lorentz violating extension of the standard model*, *Phys. Rev. D* **58** (1998) 116002 [\[hep-ph/9809521\]](#).
- [26] V. A. Kostelecky, *Gravity, Lorentz violation, and the standard model*, *Phys. Rev. D* **69** (2004) 105009 [\[hep-th/0312310\]](#).
- [27] M. Mewes, *Lorentz Violation, Electrodynamics, and the Cosmic Microwave Background*, in *4th Meeting on CPT and Lorentz Symmetry*, pp. 23–29, 2008, DOI [\[0804.0269\]](#).
- [28] A. Lue, L.-M. Wang and M. Kamionkowski, *Cosmological signature of new parity violating interactions*, *Phys. Rev. Lett.* **83** (1999) 1506 [\[astro-ph/9812088\]](#).
- [29] L. Caloni, S. Giardiello, M. Lembo, M. Gerbino, G. Gubitosi, M. Lattanzi et al., *Probing Lorentz-violating electrodynamics with CMB polarization*, *JCAP* **03** (2023) 018 [\[2212.04867\]](#).
- [30] J. P. Kaufman, B. G. Keating and B. R. Johnson, *Precision Tests of Parity Violation over Cosmological Distances*, *Mon. Not. Roy. Astron. Soc.* **455** (2016) 1981 [\[1409.8242\]](#).
- [31] Y. Minami and E. Komatsu, *New Extraction of the Cosmic Birefringence from the Planck 2018 Polarization Data*, *Phys. Rev. Lett.* **125** (2020) 221301 [\[2011.11254\]](#).
- [32] P. Diego-Palazuelos et al., *Cosmic Birefringence from Planck Public Release 4*, in *56th Rencontres de Moriond on Cosmology*, 3, 2022, [2203.04830](#).
- [33] P. Diego-Palazuelos and E. Komatsu, *Cosmic Birefringence from the Atacama Cosmology Telescope Data Release 6*, [2509.13654](#).
- [34] W. W. Yin, L. Dai, J. Huang, L. Ji and S. Ferraro, *New Probe of Cosmic Birefringence Using Galaxy Polarization and Shapes*, *Phys. Rev. Lett.* **134** (2025) 161001 [\[2402.18568\]](#).
- [35] G. Orlando, T. Flöss, P. D. Meerburg and J. Silk, *Local non-Gaussianities from cross-correlations between the CMB and 21-cm bispectrum*, *Phys. Rev. D* **112** (2025) 043523 [\[2307.15046\]](#).
- [36] S. Tanaka, S. Yoshiura, K. Kubota, K. Takahashi, A. J. Nishizawa and N. Sugiyama, *Detectability of CMB Weak Lensing and HI Cross Correlation and constraints on cosmological parameters*, [1904.10363](#).
- [37] L. Ji, S. C. Hotinli and M. Kamionkowski, *Cross-correlation of the polarizations of the 21-cm and cosmic microwave backgrounds*, *Phys. Rev. D* **107** (2023) 123533 [\[2110.01619\]](#).
- [38] K. Kadota, J. Ooba, H. Tashiro, K. Ichiki and G.-C. Liu, *Cross-correlation between 21-cm radiation and CMB B modes from the cosmic birefringence in the presence of a light scalar field*, *Phys. Rev. D* **100** (2019) 063506 [\[1906.00721\]](#).

- [39] PLANCK collaboration, *Planck 2018 results. VI. Cosmological parameters*, *Astron. Astrophys.* **641** (2020) A6 [[1807.06209](#)].
- [40] A.-S. Deutsch, M. C. Johnson, M. Münchmeyer and A. Terrana, *Polarized Sunyaev Zel'dovich tomography*, *JCAP* **04** (2018) 034 [[1705.08907](#)].
- [41] E. D. Kovetz et al., *Line-Intensity Mapping: 2017 Status Report*, [1709.09066](#).
- [42] Y. Ali-Haïmoud, P. D. Meerburg and S. Yuan, *New light on 21 cm intensity fluctuations from the dark ages*, *Phys. Rev. D* **89** (2014) 083506 [[1312.4948](#)].
- [43] R. Mondal and R. Barkana, *Prospects for precision cosmology with the 21 cm signal from the dark ages*, *Nature Astron.* **7** (2023) 1025 [[2305.08593](#)].
- [44] S. Singh, J. Nambissan T., R. Subrahmanyam, N. Udaya Shankar, B. S. Girish, A. Raghunathan et al., *On the detection of a cosmic dawn signal in the radio background*, *Nature Astron.* **6** (2022) 607 [[2112.06778](#)].
- [45] G. Facchinetto, L. Lopez-Honorez, Y. Qin and A. Mesinger, *21cm signal sensitivity to dark matter decay*, *JCAP* **01** (2024) 005 [[2308.16656](#)].
- [46] L. Lopez-Honorez, O. Mena, A. Moliné, S. Palomares-Ruiz and A. C. Vincent, *The 21 cm signal and the interplay between dark matter annihilations and astrophysical processes*, *JCAP* **08** (2016) 004 [[1603.06795](#)].
- [47] A. Hall, C. Bonvin and A. Challinor, *Testing General Relativity with 21-cm intensity mapping*, *Phys. Rev. D* **87** (2013) 064026 [[1212.0728](#)].
- [48] B. R. Dinda, M. W. Hossain and A. A. Sen, *21-cm power spectrum in interacting cubic Galileon model*, *J. Astrophys. Astron.* **44** (2023) 85 [[2208.11560](#)].
- [49] B. Joshi and R. Kothari, *Constraining statistical isotropy using 21 cm power spectrum and bispectrum*, *JCAP* **08** (2025) 047 [[2502.10717](#)].
- [50] M. Shiraishi, J. B. Muñoz, M. Kamionkowski and A. Raccanelli, *Violation of statistical isotropy and homogeneity in the 21-cm power spectrum*, *Phys. Rev. D* **93** (2016) 103506 [[1603.01206](#)].
- [51] B. Li, Z. Chen, Y.-F. Cai and Y. Mao, *Testing the scale-dependent hemispherical asymmetry with the 21-cm power spectrum from the epoch of reionization*, *Mon. Not. Roy. Astron. Soc.* **487** (2019) 5564 [[1904.04683](#)].
- [52] A. Hussain, S. Thakur, T. Guha Sarkar and A. A. Sen, *Prospects of probing quintessence with HI 21-cm intensity mapping survey*, *Mon. Not. Roy. Astron. Soc.* **463** (2016) 3492 [[1603.02087](#)].
- [53] P.-J. Wu and X. Zhang, *Prospects for measuring dark energy with 21 cm intensity mapping experiments*, *JCAP* **01** (2022) 060 [[2108.03552](#)].
- [54] C. G. Sabiu, K. Kadota, J. Asorey and I. Park, *Probing ultra-light axion dark matter from 21 cm tomography using Convolutional Neural Networks*, *JCAP* **01** (2022) 020 [[2108.07972](#)].
- [55] H. Padmanabhan, A. Refregier and A. Amara, *Cross-correlating 21 cm and galaxy surveys: implications for cosmology and astrophysics*, *Mon. Not. Roy. Astron. Soc.* **495** (2020) 3935 [[1909.11104](#)].
- [56] F. Lepori, E. Di Dio, E. Villa and M. Viel, *Optimal galaxy survey for detecting the dipole in the cross-correlation with 21 cm Intensity Mapping*, *JCAP* **05** (2018) 043 [[1709.03523](#)].
- [57] M. Zaldarriaga and U. Seljak, *An all sky analysis of polarization in the microwave background*, *Phys. Rev. D* **55** (1997) 1830 [[astro-ph/9609170](#)].
- [58] U. Seljak and M. Zaldarriaga, *A Line of sight integration approach to cosmic microwave background anisotropies*, *Astrophys. J.* **469** (1996) 437 [[astro-ph/9603033](#)].

- [59] N. Bartolo, S. Matarrese, M. Peloso and A. Ricciardone, *Anisotropic power spectrum and bispectrum in the  $f(\phi)F^2$  mechanism*, *Phys. Rev. D* **87** (2013) 023504 [[1210.3257](#)].
- [60] A. Vahedi, J. Khodagholtzadeh, R. Mohammadi and M. Sadegh, *Generation of Circular Polarization of CMB via Polarized Compton Scattering*, *JCAP* **01** (2019) 052 [[1809.08137](#)].
- [61] M. Sadegh, R. Mohammadi and I. Motie, *Generation of circular polarization in CMB radiation via nonlinear photon-photon interaction*, *Phys. Rev. D* **97** (2018) 023023 [[1711.06997](#)].
- [62] E. T. Newman and R. Penrose, *Note on the Bondi-Metzner-Sachs group*, *J. Math. Phys.* **7** (1966) 863.
- [63] K. M. Smith, W. Hu and M. Kaplinghat, *Cosmological Information from Lensed CMB Power Spectra*, *Phys. Rev. D* **74** (2006) 123002 [[astro-ph/0607315](#)].
- [64] L. Ji, S. C. Hotinli and M. Kamionkowski, *Cross-correlation of the polarizations of the 21-cm and cosmic microwave backgrounds*, *Phys. Rev. D* **107** (2023) 123533 [[2110.01619](#)].
- [65] V. Gluscevic and M. Kamionkowski, *Testing Parity-Violating Mechanisms with Cosmic Microwave Background Experiments*, *Phys. Rev. D* **81** (2010) 123529 [[1002.1308](#)].
- [66] A. Mesinger, ed., *The Cosmic 21-cm Revolution*, 2514-3433. IOP Publishing, 2019, [10.1088/2514-3433/ab4a73](#).
- [67] S. Furlanetto, S. P. Oh and F. Briggs, *Cosmology at Low Frequencies: The 21 cm Transition and the High-Redshift Universe*, *Phys. Rept.* **433** (2006) 181 [[astro-ph/0608032](#)].
- [68] S. Bharadwaj and S. S. Ali, *The CMBR fluctuations from HI perturbations prior to reionization*, *Mon. Not. Roy. Astron. Soc.* **352** (2004) 142 [[astro-ph/0401206](#)].
- [69] N. Kaiser, *Clustering in real space and in redshift space*, *MNRAS* **227** (1987) 1.
- [70] D. Babich and A. Loeb, *Polarization of 21cm radiation from the epoch of reionization*, *Astrophys. J.* **635** (2005) 1 [[astro-ph/0505358](#)].
- [71] B. Li, J. Tan and Y. Mao, *Linear Polarization of the 21 cm Line from the Epoch of Reionization*, *Astrophys. J.* **918** (2021) 14 [[2101.11543](#)].
- [72] L. Ji, S. C. Hotinli and M. Kamionkowski, *Cross-correlation of the polarizations of the 21-cm and cosmic microwave backgrounds*, *Phys. Rev. D* **107** (2023) 123533 [[2110.01619](#)].
- [73] Y. Gong, X. Chen, M. Silva, A. Cooray and M. G. Santos, *The OH line contamination of 21 cm intensity fluctuation measurements for  $z=1\sim4$* , *Astrophys. J. Lett.* **740** (2011) L20 [[1108.0947](#)].
- [74] D. Karagiannis, R. Maartens, S. Saito, J. Fonseca, S. Camera and C. Clarkson, *Squeezing information from radio surveys to probe the primordial Universe*, [2406.00117](#).
- [75] M. G. Santos et al., *Cosmology from a SKA HI intensity mapping survey*, *PoS AASKA14* (2015) 019 [[1501.03989](#)].
- [76] P. Bull, P. G. Ferreira, P. Patel and M. G. Santos, *Late-time cosmology with 21cm intensity mapping experiments*, *Astrophys. J.* **803** (2015) 21 [[1405.1452](#)].
- [77] R. Durrer, M. Jalilvand, R. Kothari, R. Maartens and F. Montanari, *Full-sky bispectrum in redshift space for 21cm intensity maps*, *JCAP* **12** (2020) 003 [[2008.02266](#)].
- [78] COSMIC VISIONS 21 CM collaboration, *Inflation and Early Dark Energy with a Stage II Hydrogen Intensity Mapping experiment*, [1810.09572](#).
- [79] D. Karagiannis, R. Maartens and L. F. Randrianjanahary, *Cosmological constraints from the power spectrum and bispectrum of 21cm intensity maps*, *JCAP* **11** (2022) 003 [[2206.07747](#)].
- [80] E. Komatsu, *New physics from the polarized light of the cosmic microwave background*, *Nature Rev. Phys.* **4** (2022) 452 [[2202.13919](#)].

- [81] PLANCK collaboration, *Planck intermediate results. XLIX. Parity-violation constraints from polarization data*, *Astron. Astrophys.* **596** (2016) A110 [[1605.08633](#)].
- [82] R. Kothari and R. Maartens, *A wide-angle formulation of foreground filters for HI intensity mapping*, *JCAP* **05** (2024) 089 [[2308.03462](#)].
- [83] M. Kopana, S. Jolicoeur and R. Maartens, *Constraining primordial non-Gaussianity by combining photometric galaxy and 21 cm intensity mapping surveys*, *Eur. Phys. J. C* **85** (2025) 538 [[2409.19383](#)].
- [84] S. J. Rossiter, S. Camera, C. Clarkson and R. Maartens, *Decoupling local primordial non-Gaussianity from relativistic effects in the galaxy bispectrum*, *JCAP* **07** (2025) 055 [[2407.06301](#)].
- [85] D. Alonso, P. Bull, P. G. Ferreira and M. G. Santos, *Blind foreground subtraction for intensity mapping experiments*, *Mon. Not. Roy. Astron. Soc.* **447** (2015) 400 [[1409.8667](#)].
- [86] M. Spinelli, I. P. Carucci, S. Cunningham, S. E. Harper, M. O. Irfan, J. Fonseca et al., *SKAO  $H_i$  intensity mapping: blind foreground subtraction challenge*, *Mon. Not. Roy. Astron. Soc.* **509** (2021) 2048 [[2107.10814](#)].
- [87] J. R. Shaw, K. Sigurdson, M. Sitwell, A. Stebbins and U.-L. Pen, *Coaxing cosmic 21 cm fluctuations from the polarized sky using  $m$ -mode analysis*, *Phys. Rev. D* **91** (2015) 083514 [[1401.2095](#)].
- [88] T. M. Oxholm and E. R. Switzer, *Intensity mapping without cosmic variance*, *Phys. Rev. D* **104** (2021) 083501 [[2107.02111](#)].
- [89] T. Chen and M. Remazeilles, *Impact of thermal Sunyaev–Zeldovich effect on cross-correlations between Planck cosmic microwave background lensing and SDSS galaxy density fields*, *Mon. Not. Roy. Astron. Soc.* **514** (2022) 596 [[2203.04809](#)].